NANO LETTERS

pubs.acs.org/NanoLett

Plasmonic Nanowire Antennas: Experiment, Simulation, and Theory

Jens Dorfmüller,[*,†] Ralf Vogelgesang,[*,†] Worawut Khunsin,[†] Carsten Rockstuhl,[‡] Christoph Etrich,[§] and Klaus Kern[†,||]

[†] Max-Planck-Institut für Festkörperforschung, Heisenbergstrasse 1, 70569 Stuttgart, Germany, [‡] Institut für Festkörpertheorie and -optik and [§] Institut für angewandte Physik, Friedrich-Schiller-Universität, Max-Wien-Platz 1, 07743 Jena, Germany, and [||] Institut de Physique de la Matière Condensée, École Polytechnique Fédérale de Lausanne, 1015 Lausanne, Switzerland

ABSTRACT Recent advances in nanolithography have allowed shifting of the resonance frequency of antennas into the optical and visible wavelength range with potential applications, for example, in single molecule spectroscopy by fluorescence and directionality enhancement of molecules. Despite such great promise, the analytical means to describe the properties of optical antennas is still lacking. As the phase velocity of currents at optical frequencies in metals is much below the speed of light, standard radio frequency (RF) antenna theory does not apply directly. For the fundamental linear wire antenna, we present an analytical description that overcomes this shortage and reveals profound differences between RF and plasmonic antennas. It is fully supported by apertureless scanning near-field optical microscope measurements and finite-difference time-domain simulations. This theory is a starting point for the development of analytical models of more complex antenna structures.

KEYWORDS Optical antenna, antenna theory, plasmonics, near-field optics, scanning near-field optical microscopy, antenna directionality

In the radio frequency and microwave regime, the antenna is a well-established concept.[1] (Semi-) analytic theories, derived from the notion of perfect conductors that carry only surface currents, continue to guide engineers in optimizing antennas for many different applications with profound impact on society. Recent developments in nanotechnology allowed shifting the resonance of antennas into the visible part of the electromagnetic spectrum.[2,3] This new class of antenna received already great attention due to its abilities of enhancing[4,5] and directing[6,7] the emission of single molecules and it bears great potential for sensing applications and small volume spectroscopy.[8,9] Coupling of specifically chosen antennas leads to novel resonance effects such as electromagnetically induced transparency[10,11] and gives rise to a new class of materials, the so-called metamaterials.[12,13]

In the process of antenna improvement, the pioneers of radio engineering developed analytical approximations, which at the same time fostered a deep intuitive understanding. Today, the design and optimization of optical antennas are largely done with generic numeric Maxwell solvers.[6,14] The larger and more complex the investigated structures, the greater are the possibilities for new fruitful discoveries—at the expense, however, of rapidly inflating computational costs for the research. The precise analysis of extended three-dimensional (3D) plasmonic systems still often exceeds current computational limits. Accurate analytical models are very welcome predictors of structure behavior and/or device performance. They ease the design and optimization processes as well as extend intuitive understanding. While the scattering of isolated plasmonic spheres as the simplest optical antennas has been solved analytically in closed form by Mie more than 100 years ago,[15] equivalent solutions for most other relevant geometries continue to be elusive.

In this paper, we present a model for another fundamental building block of plasmonic antennas, the linear thin wire element. It explains the excitation of such wires by far-field sources for both, on- and off-resonance conditions and provides information regarding the amplitude and phase of the radiation scattered in arbitrary directions. It also predicts the scattering and directivity of the antennas and has the potential to simplify modeling of multiwire structures, such as Yagi-Uda composites.[6,7,16,17] At its heart, this theory describes the longitudinal resonances of the fundamental transversal wire mode. These longitudinal resonances arise from the finite length of the wires discretizing the continuous mode spectrum and lead to Fabry-Pérot resonances. Contributions from higher order transversal modes are subsumed in a small signal offset when fitting our experimental/numerical results with predictions from the analytical model. In deriving the model, we let us guide by textbook RF antenna theory as far as possible.[18,19] With the skin depth being of the same order as the antenna diameter and larger,[20] however, the assumption of surface currents clearly cannot be upheld. Instead, the fields occupy the bulk of the antenna and justify our assumption of a homogeneous volume current. Ultimately, this seemingly small modification fully describes the drastically altered coupling behavior

* To whom correspondence should be addressed: E-mail: (J.D.) J.Dorfmueller@fkf.mpg.de; (R.V.) R.Vogelgesang@fkf.mpg.de.
Received for review: 05/31/2010
Published on Web: 08/20/2010

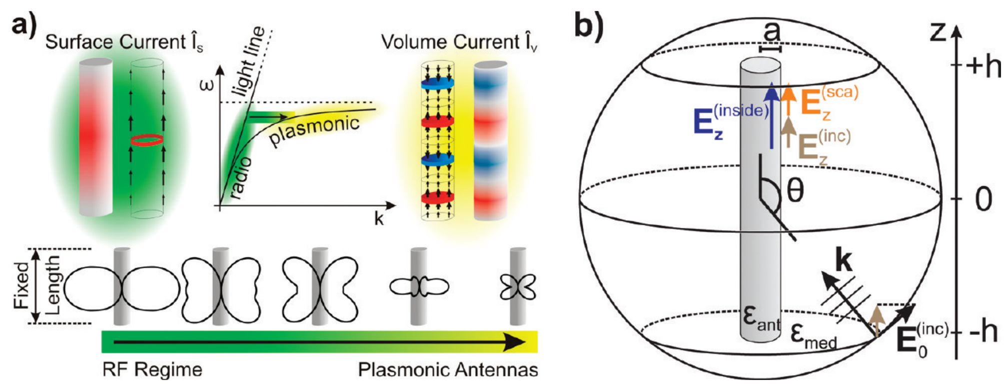

FIGURE 1. (a) Contrasting RF and plasmonic antenna theory. RF antenna theory with only a surface current (left) and plasmonic antenna theory with a volume current (right) that leads to a much shorter (plasmon) wavelength as it can be seen in the dispersion relation (center). Transferring a fixed length antenna from the RF regime to the plasmonic regime leads to fundamentally different radiation patterns (bottom). (b) Geometry of the illuminating field. The component parallel to the wire of the incidence *E*-field $E_z^{(inc)}$ is responsible for exciting the longitudinal resonances in the wire.

of plasmonic antennas to the free space radiation, as indicated pictorially at the bottom of Figure 1a.

Our model is verified with data obtained by apertureless Scanning Near-field Optical Microscope (aSNOM)[21] and finite-difference time-domain (FDTD) simulations.[22] As we showed previously, the near-field amplitude recorded by cross-polarization aSNOM can be used to map the resonant responses of single plasmonic antennas,[23] which strongly depend on the illumination direction and may even be entirely forbidden under certain conditions such as even order modes are under perpendicular illumination. With this angle dependence, essentially reflecting the directivity of the antennas, we can extract the receiving patterns from our data. The extensive sets of measured and simulated data covering the complete interval of azimuthal angles we present here can be interpreted by our powerful yet simple model with only a handful of physically motivated parameters. The excellent agreement of the model with simulations and experiments instills confidence in a wide range of applicability for this model.

Analytical Model. To obtain insightful, easy to comprehend analytical expressions, we consider cylindrical wires with a diameter much smaller than the wavelength and skin depth. The exact diameter and cross-sectional geometry enters only indirectly through the (complex valued) plasmon propagation constant of the wire mode k_p that is chosen to accurately reflect the mode constant of the substrate supported wire.[24] We treat the surrounding medium to be vacuum ($\varepsilon_{med} = \varepsilon_0$). Note that throughout this manuscript we use *absolute* unit-bearing dielectric constants, not relative values. The excitation of our wires, which will be described as currents induced in the wires, depends on the direction and polarization of the illuminating electromagnetic field.

Our illumination geometry is shown in Figure 1b. The cylindrical wire with permittivity ε_{ant}, radius a, and length $l = 2h$ is aligned parallel to the z-axis and placed in the center of the coordinate system. Right at the wire surface the three relevant E-fields (the incident $\mathbf{E}^{(inc)}$, the scattered $\mathbf{E}^{(sca)}$, and the field inside of the wire $\mathbf{E}^{(inside)}$) fulfill the boundary condition $E_z^{(inc)} + E_z^{(sca)} = E_z^{(inside)}$. As the end facets are small compared to the cylinder's side, we neglect them, anticipating that wire end effects will not be explained by the model and require an ad hoc parameter.

Assuming a p-polarized plane wave with field strength $E_0^{(inc)}$ and wave vector $\mathbf{k}$ impinging on the wire at an angle of incidence θ, we find the field component that drives the plasmonic response:

$$E_z^{(inc)}(z) = E_0^{(inc)} \sin\theta\, e^{ik\cos\theta z} \qquad (1)$$

In the thin-wire limit, it depends only on z but not on the equatorial coordinates.

The same holds for the induced current density inside the plasmonic metal wire,[25] which we approximate as homogeneous over the wire cross section: $\mathbf{I}(\mathbf{x}) = I_z(z)\mathbf{e}_z$. At 800 nm excitation wavelength, for instance, in the fundamental mode of a gold wire of a 20 nm diameter, the current density varies less than 5% across the wire. The scattered field $E_z^{(sca)}$ associated with this current density, can be expressed by a vector potential $\mathbf{A}(\mathbf{x})$.[18,19] Together with harmonic time dependence $e^{-i\omega t}$ (where ω is the angular frequency of the time harmonic electrical field), in cylindrical coordinates and Lorenz gauge, it reads

$$\mathbf{A}_z(z, r, \phi) = \frac{\mu_0}{4\pi}\int_{V'} I_z(z')\frac{e^{ikR}}{R}\mathrm{d}^3x' = \frac{\mu_0}{4\pi}\int_{-h}^{h} I_z(z')G(z - z', r)\mathrm{d}z' \qquad (2)$$

where $R = |\mathbf{x} - \mathbf{x}'|$, V' is the wire volume, and $G(z - z', r)$ is the thin wire kernel.[19]

At this point, we adopt Pocklington's ansatz[26] for the kernel evaluation at the wire surface, $G(z - z', r = a) \approx \tilde{Z}\delta(z$

DOI: 10.1021/nl101921y | Nano Lett. 2010, 10, 3596–3603

$- z')$, where $\tilde{Z}$ takes the role of a characteristic impedance of the wire. Crude as this approximation might seem at first, it is fully justified by our observations, and it has the tremendous appeal of being fully analytical. In stark contrast, exact solutions of the integral (i.e., Hallén's method of iteration[27]) would require numerical efforts to solve it. We obtain for the scattered E-field outside the wire[18]

$$E_z^{(\mathrm{sca})}(z,a) = \frac{ic^2}{\omega}\left(\frac{\partial^2}{\partial z^2} + k^2\right)\mathbf{A}_z(z,a) = \frac{ic^2}{\omega}\left(\frac{\partial^2}{\partial z^2} + k^2\right)\frac{\mu_0}{4\pi}\tilde{Z}I_z(z) \quad (3)$$

While the previous steps closely followed RF antenna theory for perfect conductors ($|\varepsilon_{\mathrm{ant}}| \to \infty$), we deviate now by allowing an electric field $\mathbf{E}^{(\mathrm{inside})}$ inside of the wire. For the current density inside of the wire we find

$$\mathbf{I}(\mathbf{x}) = \sigma\mathbf{E}^{(\mathrm{inside})}(\mathbf{x}) = \omega\ \mathrm{Im}(\varepsilon_{\mathrm{ant}})\mathbf{E}^{(\mathrm{inside})}(\mathbf{x}) \quad (4)$$

In the thin-wire limit, this current density is nearly homogeneous, as can be illustrated with the analytic case of circular cross sections; the fundamental mode is rotationally symmetric and $E_\phi = 0$. For the other E-field components, we can find an approximation for small radii, $|ka| \ll 1$, from analytical calculations of the fundamental plasmon mode ($n = 0$) of an infinitely long cylinder.[28−30] The radial component is described by a first order Bessel function $E_{\mathrm{r}}^{(\mathrm{inside})} \propto J_1(k_{\mathrm{r}}r)$, where k_{r} is the radial wavenumber. It can be neglected in comparison to the longitudinal field component, described by a zeroth order Bessel function $E_z^{(\mathrm{inside})} \propto J_0(k_{\mathrm{r}}r)$. For small radii a, we may thus regard $E_z^{(\mathrm{inside})}$ as constant and obtain for the current density

$$I_z(z) = \omega\ \mathrm{Im}(\varepsilon_{\mathrm{ant}})E_z^{(\mathrm{inside})}(z) \quad (5)$$

The three equations of the tangential E-field components 1, 3, and 5 combine to an inhomogeneous differential equation for the current density $I_z(z)$ in which $E_z^{(\mathrm{inc})}(z)$ plays the intuitive role of an external driving term. We solve this equation by the following ansatz

$$I_z(z) = I_{\|}e^{ik_{\|}z} + I_{\pm p}e^{\pm ik_{\mathrm{p}}z} + I_{\pm}e^{\pm ikz} \quad (6)$$

This ansatz assumes five different current waves traveling along the wire: First, a current density $I_{\|}e^{ik_{\|}z}$ induced by the illuminating field with the same wave vector along the wire ($k_{\|} = k\cos\theta$); second, two counter-propagating plasmonic current densities $I_{+p}e^{+ik_{\mathrm{p}}z}$ and $I_{-p}e^{-ik_{\mathrm{p}}z}$, which are not included in RF antenna theory but have to be expected as the electronic part of plasmonic modes known to exist on wires;[28,29] last, for completeness' sake and self-consistency checking, we include the two standard terms of RF antenna theory (e.g., refs 19 and 31) I_+e^{+ikz} and I_-e^{-ikz}, which represent waves traveling along the wire with vacuum speed of light. However, inserting this ansatz and comparing the prefactors immediately forces one to set $I_+ = I_- = 0$. In contrast to RF antenna theory, plasmonic antennas cannot support currents with vacuum phase velocity. Somewhat surprisingly the following is also directly obtained

$$\tilde{Z} = \frac{4\pi\varepsilon_0 i}{\mathrm{Im}(\varepsilon_{\mathrm{ant}})(k_{\mathrm{p}}^2 - k^2)} \quad (7)$$

$$I_{\|} = \omega\ \mathrm{Im}(\varepsilon_{\mathrm{ant}})\frac{(k_{\mathrm{p}}^2 - k^2)\sin\theta}{k_{\mathrm{p}}^2 - k^2\cos^2\theta}E_0^{(\mathrm{inc})} \quad (8)$$

In antenna theory, $\tilde{Z}$ is akin to the antenna impedance and has to be calculated separately. Here it assumes a natural role as characteristic mode impedance.

At this point, we have to consider the role of the wire endcaps. As mentioned above, their influence is not amenable to simple analytic description,[32] but they are well understood. To the free charges inside the wire, they are a hard boundary at which the total current density has to vanish, leading to:

$$I_{\pm p} = -I_{\|}\frac{\sin((k_{\mathrm{p}} \pm k\cos\theta)h)}{\sin(2k_{\mathrm{p}}h)} \quad (9)$$

The electromagnetic fields, however, are not required to vanish at the physical wire ends. Indeed, their penetration into the surrounding medium lets the wire mode pick up an additional phase upon reflection, as if the wire length increases by $l_{\mathrm{reactance}}$, so that we substitute $h \to (l + l_{\mathrm{reactance}})/2$ in our equations.[33] This "apparent length increase" has already been appreciated in RF antenna theory of microstrip antennas,[34] where it is often formulated as a reactance in equivalent electronic circuits. For plasmonic nanoantennas, it cannot be neglected even for thin wires.[23,32] Finally, the influence of all higher order transversal wire modes that do couple to the exciting radiation is captured by an offset E_{offset}, which will, in general, vary with the illumination angle θ. From the currents as calculated with these simple analytical expression all quantities of interest can be derived.

Verification of the Model. The current excited in an optical antenna can be probed indirectly, for example, with microbolometers[35] or two-photon-luminescence.[2,36] Here,

DOI: 10.1021/nl101921y | Nano Lett. 2010, 10, 3596–3603

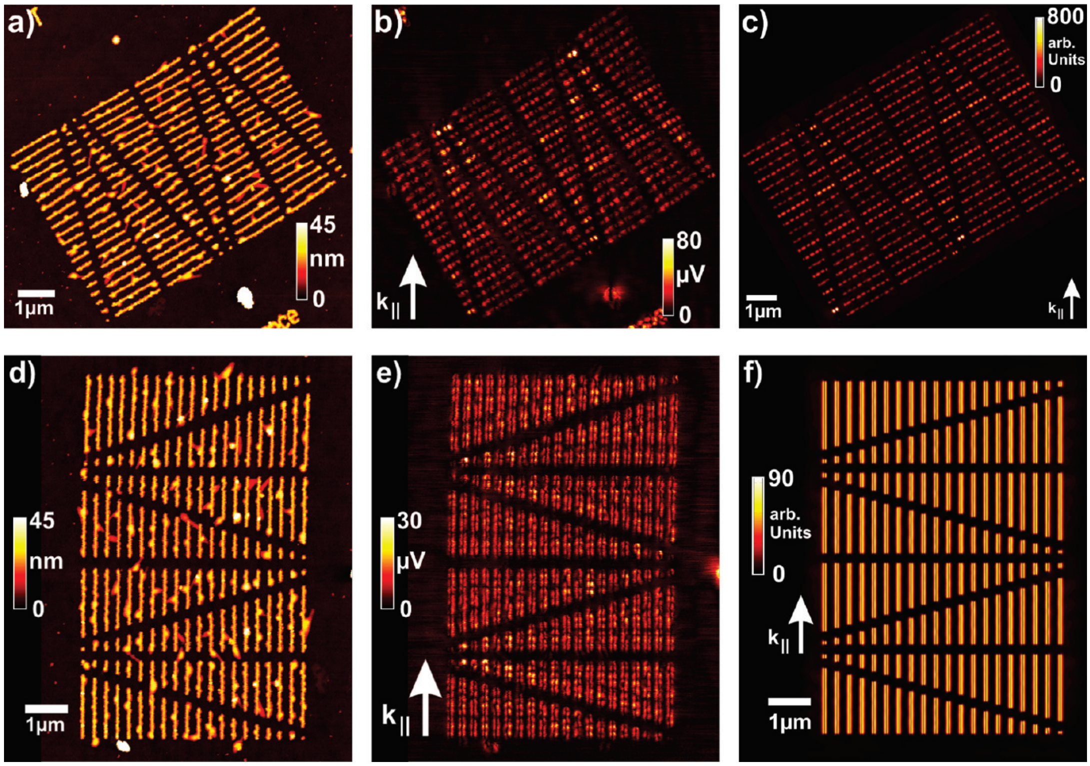

FIGURE 2. Near-field images of plasmonic wire antennas illuminated by a 911 nm wavelength illumination laser beam from different directions. (a−c) $\theta = 60°$ and (d−f) $\theta = 0°$. The length of the 40 nm wide and 25 nm high gold wires on a SiO_2 surface varies from 40 to 1630 nm across the structure. (a,d) The noncontact AFM topography, (b,e) the simultaneously measured aSNOM near-field signal, and (c,f) the according magnitude of the normal component of the E-field 24 nm above the structure obtained from FDTD simulations. Note: the signal in (b,c,e,f) exactly above the wire is equal to the radial component E_r.

we use measured near-field images obtained by cross-polarized aSNOM and simulated near-field images obtained by FDTD to determine the response of individual antennas (see Figure 2). The former has the advantage of imposing very little perturbation on plasmonic eigenmodes and offers direct maps of the normal E-field component near the measured nanostructures.[23,37] Above the center of the wire, this component is equal to the radial component E_r that can be extracted for thin wires from our model as $E_r^{(\mathrm{outside})}(a) \approx -(a\varepsilon_{\mathrm{ant}})/(2\omega\varepsilon_{\mathrm{med}}\ \mathrm{Im}(\varepsilon_{\mathrm{ant}}))/\partial_z I_z$ (see Supporting Information).

In Figure 3a−d the simulated amplitude and phase near-field images of the first and third order resonant wires are shown as obtained by the FDTD method. The first order images show two lobes with a 180° phase difference and a node in between them. This is also reflected in the line-cuts of Figure 3e,f, showing that the theory of a first order resonant wire can model this behavior very well in both amplitude and phase by matching the analytical expressions to the measured radial field by adjusting the free parameters k_p and $E_0^{(\mathrm{inc})}$ plus a phase offset reflecting the phase of the excitation field. The model of the third order resonant wire in Figure 3g,h nicely recovers the four lobes with three nodes in between as well as the phase difference between neighboring lobes.

Next we ask, whether our model is able to explain Fabry-Pérot resonances of the nanowires.[23] To this end, we extract maximum amplitude plots from near-field images of many wires of different lengths, which immediately reveal several geometric resonances. Typical examples are shown for experiment and simulation in Figure 4. A slightly oblique illumination scheme is taken into account by suitable coordinate transformation (see Supporting Information).

For a given wavelength, a cylindrical cross-section and a homogeneous surrounding medium the parameters k_p and $l_{\mathrm{reactance}}$ can be obtained from numerical solutions of the pertinent transcendental equation[28−30,32] or from approximated analytical expressions.[38] For wires of arbitrary cross-sectional shape on a surface, one needs numerical mode solvers. In the present case, we treat k_p, $l_{\mathrm{reactance}}$, E_{offset}, and $E_0^{(\mathrm{inc})}$ as free parameters and are able to fit all our data. The red curves in Figure 4 show the remarkable agreement between the model and experiment/simulation. Slight deviations at lengths shorter than the dipole resonance ($l < \pi/k_p$) are due to the use of a simplified fitting procedure, which considers incoherent sums of the partial currents to lighten the numerical burden (see Supporting Information).

The simulation for the rotation angle of $\theta = 0°$ (see Figure 4f) shows no significant peaks and the data points deviate only little from the constant E_{offset}. In the near-field image in Figure 2f, we identify a clear signal contribution from higher order transversal modes, but essentially no signal due to the fundamental mode. We attribute the less than perfect sup-

DOI: 10.1021/nl101921y | Nano Lett. 2010, 10, 3596--3603

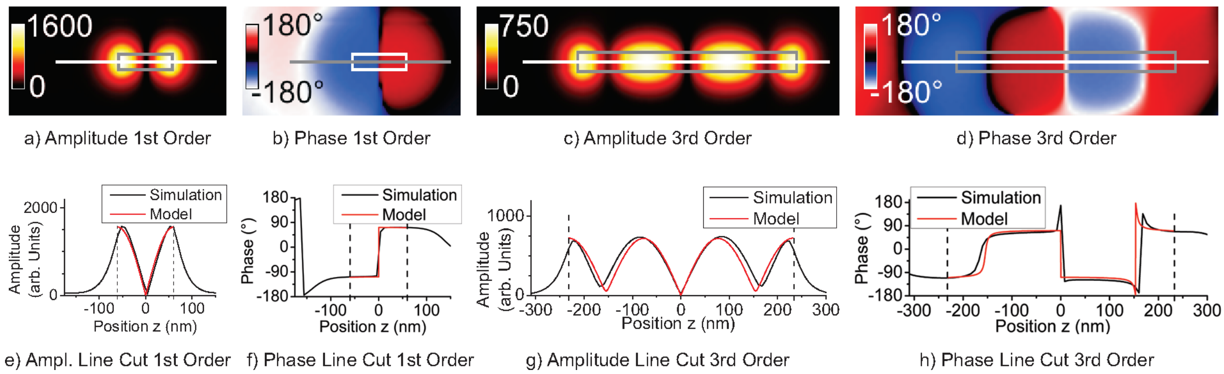

FIGURE 3. Comparisons between simulated near-field images and the model's radial E-field component for the first and third order wire resonance. (a−d) The amplitude and phase of the z-component of the E-field 24 nm above the sample. The rectangles indicate the position of the wires, and the lines indicate where the line cuts used in (e−h) have been taken.

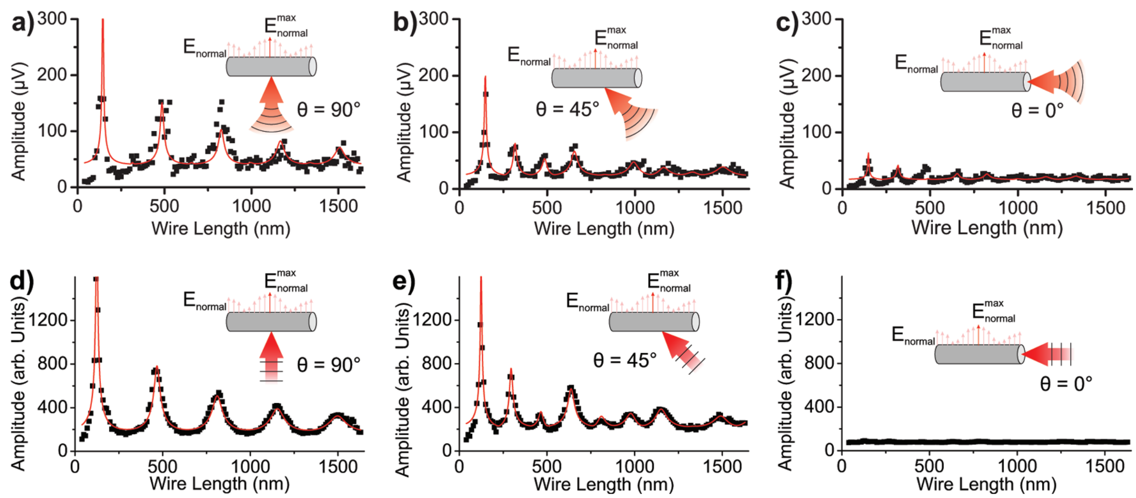

FIGURE 4. Fitting the geometric Fabry-Pérot resonances of linear wire antennas illuminated by a 911 nm wavelength laser beam. The squares show the maximum of the measured near-field amplitude above the wire for different illumination angles: (a) $\theta = 90°$, (b) $\theta = 45°$, and (c) $\theta = 0°$ while the red curve shows a fit of the E_r-field of an approximate model. (d−f) show the same for the FDTD simulation data. The squares indicate the maximum amplitude of the normal E-field component 24 nm above the wire.

TABLE 1. Comparison of Fitting Parameters

	$\lambda_p = 2\pi/\mathrm{Re}(k_p)$	$\mathrm{Im}(k_p)$	$l_{reactance}$
experiment	337.5 nm	0.387 μm^{-1}	22.20 nm
simulation	342.9 nm	0.498 μm^{-1}	47.12 nm

pression observed in the experimental results in Figures 2e and 4c to experimental imperfections.

Our model successfully represents not only data for single illumination angles very well, but allows a total fit to the complete data sets consisting of 160 wires illuminated in experiment and simulation from 7 and 19 different angles, respectively. The resulting values of the three angle independent parameters are listed in Table 1. While in simulations the excitation amplitude $E_0^{(inc)}$ is also independent of illumination angle, variations in laser power and other experimental conditions necessitate the use of a different $E_0^{(inc)}$ for each near-field image.

The agreement in plasmon wavelength λ_p between experiment and simulation is excellent. To our surprise, the plasmon damping is even smaller in experiment than in simulation, even though we use thermally evaporated gold and compare it to the permittivity obtained by Johnson and Christy[39] used in the simulation. One could speculate that slightly thicker wires in the experiment are causing this behavior. The influence of the shape of the wire termination (slightly rounded electron-beam written ones in the experiment and flat ends in FDTD simulation) might also have an influence on the strength of the losses as well as on the apparent length increase $l_{reactance}$.

Applying the Model. As a first application of the model, we use it to explain the systematic differences that we observed between simulation and experiment. Figure 5a compares the resonances for an illumination angle $\theta = 15°$. While in the simulated data the third and the sixth order resonance peaks are missing, a much stronger eighth order resonance appears than for the experimental data. We suspect the use of different illumination geometries (focused vs plane wave illumination) causes these deviations.

By using our model with the illumination angle as an additional fitting parameter, we extract its dependence on the nominal angle (see Figure 5b). While the simulation follows the

DOI: 10.1021/nl101921y | Nano Lett. 2010, 10, 3596–3603

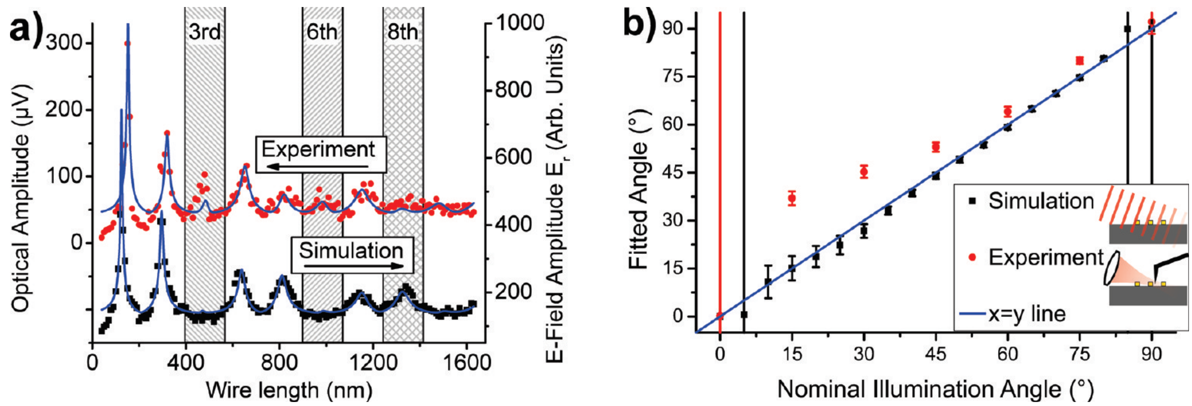

FIGURE 5. Influence of the illumination geometry. (a) Comparing resonances for $\theta = 15°$, (b) retrieving the illumination direction by the fitting algorithm.

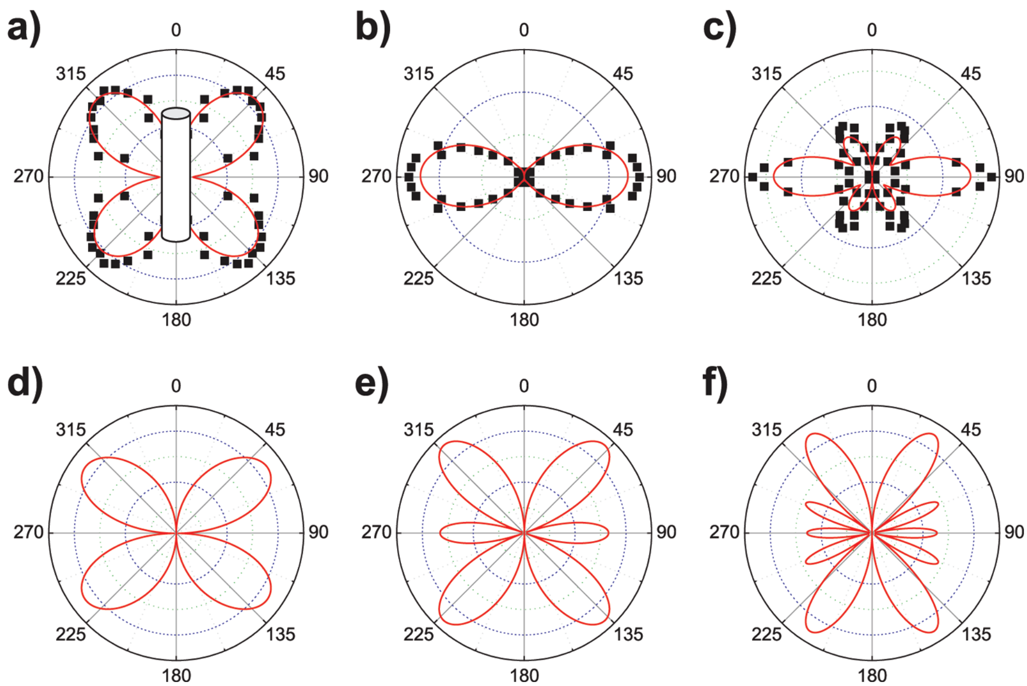

FIGURE 6. Comparison between the emission patterns of plasmonic and RF antennas. (a−c) The emission patterns of the second, third, and fifth order resonant plasmonic antennas. The dots are the heights of the resonant peaks in the geometric resonance curves of the simulation. (d−f) The emission patterns of the according RF-antennas.

$x = y$ line, the experiment deviates from it for small θ. Bearing in mind that a Gaussian focus can be described in angular spectrum representation[40] as an integral over a nearly Gaussian angular distribution of plane waves, the weaker coupling of the small angle illuminations (see eq 1) leads to the resonance curve being influenced more strongly at larger angles (see Supporting Information). At $\theta = 90°$, the symmetry of the illumination neutralizes this effect. Using the coherent sum of different angle resonance curves weighted with a Gaussian distribution and fitting the outcome with the plane wave model confirms this trend. That is, the differences between focused-beam excited experiment and plane-wave excited simulation corroborate our model.

In a second application, we look at the emission pattern of antennas. The model addresses the question of the angle dependence of the excitability of a nanoantenna which is, according to the Rayleigh-Carson reciprocity theorem,[41] equal to its emission pattern. This opens up a much larger scope for our model than just interpreting near-field measurements. It can for example be used to calculate the emission pattern of a quantum dot or a molecule coupled to nanorods.[42−44]

In Figure 6a−c, we use our model to plot the reception/emission patterns of resonant plasmonic antennas at the second, third, and fifth order resonance. The antennas are oriented vertically in these plots and we plot the field strength E. The squares are the peak heights of the respective resonance taken from the geometric resonance curves (see Figure 4). In Figure 6d−f, we plot the equivalent RF antenna emission patterns (see, e.g., refs 26 and 31).

DOI: 10.1021/nl101921y | *Nano Lett.* **2010,** *10,* 3596–-3603

The second order resonance shows the familiar quadrupole emission pattern. The difference between the RF and the plasmonic regime are very subtle with the main difference lying in the direction of the main emission. While the third order RF mode has six lobes, the side lobes of the plasmonic antenna are so very weak that it resembles a dipole. The RF emission pattern shows a trend of $2n$ lobes for the nth order resonance with the lobes closest to the wire axis being the strongest. The trend to more lobes with higher order resonances is also apparent for plasmonic antennas. Nevertheless, they clearly deviate from the $2n$ rule due to the mismatch of k and k_p along the length of the antenna. The odd order modes emit strongest always into the direction perpendicular to the wire antenna. The even order modes, in contrast, have here always a minimum due to symmetry[45] and the two lobes neighboring this minimum are always the strongest. These drastic qualitative differences that we observe justify the usage of the term "plasmonic antenna" to distinguish them from regular RF antennas.

Summary and Outlook. We presented an analytical model to describe plasmonic antennas, which can be neither described by the existing theories for perfect conductor antennas nor by the ones for dielectric materials.[46,47] In contrast to the RF regime, at optical wavelengths antennas cannot be described by a surface current only. We therefore choose the other extreme and assume a constant volume current to derive an analytic model. As long as the wire antenna is thin compared to the free space wavelength, its coupling to electromagnetic waves can be described by an ansatz of one-dimensional line currents consisting of three terms.

The approximations introduced to keep the model analytical are justified by excellent agreement with data obtained from experimental near-field images and FDTD simulations. The significant amount of high quality data allowed us to verify essential aspects of the model: near-field properties of the antennas, Fabry-Pérot resonances, and reception and emission patterns. As the agreement is not limited to the resonant wires, it allows also to calculate emission patterns for off-resonant wires and even the transition from plasmonic to RF wire antennas (see Figure 1a).

Having obtained the currents induced by electromagnetic fields, it is easy enough to expand the theory to cover the whole scattering process by calculating the reemitted light with the well-known formula for the vector potential.[18] In the far-field limit, we can reduce the equation to an analytically solvable line integral

$$\lim_{kr\to\infty}\mathbf{A}(r,\eta,\phi)=\frac{\mu_0 a^2}{4}\frac{e^{ikr}}{r}\mathbf{e}_z\int_{-h}^{h}I_z(z')e^{-ikz'\cos\eta}\mathrm{d}z' \tag{10}$$

In conjunction with this formula, it is possible to formulate an analytic scattering theory of thin linear wire antennas that is analogous to the Mie theory for spheres.

With the currents being complex valued, we can calculate the directionality, amplitude, and phase of the scattered light. This is crucial for the analytical description of more complex structures. For instance, in curtain antennas and antenna arrays consisting of equal length antennas the phase difference of light emitted by different elements is determined by distance retardation only, but passive off-resonant elements have retarding properties on their own. This plays a major role in the antenna design, for example, for the directors and reflectors in Yagi-Uda antennas.

Acknowledgment. J.D. and R.V. would like to thank Nader Engheta for stimulating discussions. The authors would like to thank R. Thomas Weitz for preparing the sample. The authors also would like to thank the anonymous referee who pointing out a small oversight in our derivation, which is inconsequential for the present letter, but would have manifested itself in spectral evaluations. The authors acknowledge support by the DFG (SPP1391) and the BMBF (METAMAT).

Supporting Information Available. A description of our methods and materials, extended derivations of equations, a discussion of how the experimental situation is considered, a description of the simplified fitting model, and the Gaussian focus analysis. This material is available free of charge via the Internet at http://pubs.acs.org.

REFERENCES AND NOTES

(1) King, R. W. P.; Fikioris, G. J.; Mack, R. B. *Cylindrical Antennas and Arrays*, 2nd ed.; Cambridge University Press: Cambridge, United Kingdom, 2002.

(2) Mühlschlegel, P.; Eisler, H.-J.; Martin, O. J. F.; Hecht, B.; Pohl, D. W. *Science* **2005**, *308*, 1607–1609.

(3) Bharadwaj, P.; Deutsch, B.; Novotny, L. *Adv. Opt. Photon.* **2009**, *1*, 438–483.

(4) Anger, P.; Bharadwaj, P.; Novotny, L. *Phys. Rev. Lett.* **2006**, *96*, 113002.

(5) Taminiau, T. H.; Stefani, F. D.; Segerink, F. B.; van Hulst, N. F. *Nat. Photonics* **2008**, *2*, 234–237.

(6) Taminiau, T. H.; Stefani, F. D.; van Hulst, N. F. *Opt. Express* **2008**, *16*, 10858–10866.

(7) Kosako, T.; Kadoya, Y.; Hofmann, H. F. *Nat. Photonics* **2010**, *4*, 312–315.

(8) Li, K.; Stockman, M. I.; Bergman, D. *Phys. Rev. Lett.* **2003**, *91*, 227402.

(9) Li, S.; Pedano, M. L.; Chang, S.-H.; Mirkin, C. A.; Schatz, G. C. *Nano Lett.* **2010**, *10*, 1722–1727.

(10) Verellen, N.; Sonnefraud, Y.; Sobhani, H.; Hao, F.; Moshchalkov, V. V.; Van Dorpe, P.; Nordlander, P.; Maier, S. A. *Nano Lett.* **2009**, *9*, 1663–1667.

(11) Liu, N.; Langguth, L.; Weiss, T.; Kästel, J.; Fleischhauer, M.; Pfau, T.; Giessen, H. *Nat. Mat.* **2009**, *8*, 758–762.

(12) Valentine, J.; Zhang, S.; Zentgraf, T.; Ulin-Avila, E.; Genov, D. A.; Bartal, G.; Zhang, X. *Nature* **2008**, *455*, 376–U32.

(13) Liu, N.; Liu, H.; Zhu, S.; Giessen, H. *Nat. Photonics* **2009**, *3*, 157–162.

(14) Huang, L.; Maerkl, S. J.; Martin, O. J. F. *Opt. Express* **2009**, *17*, 6018–6024.

(15) Mie, G. *Ann. Phys.* **1908**, *25*, 377–445.

(16) Yagi, H. *Proc. IRE* **1928**, *16*, 715–741.

(17) Li, J.; Salandrino, A.; Engheta, N. *Phys. Rev. B* **2007**, *76*, 245403.
(18) Jackson, J. D. *Classical Electrodynamics*, 3rd ed.; Wiley: New York, 1999.
(19) Orfanidis, S. J. *Electromagnetic Waves and Antennas*; Rutgers University: Piscataway, NJ, 2008.
(20) Qiang, R.; Chen, R. L.; Chen, J. *Int. J. Infrared Millimeter Waves* **2004**, *25*, 1263–1270.
(21) Bek, A.; Vogelgesang, R.; Kern, K. *Rev. Sci. Instrum.* **2006**, *77*, No. 043703.
(22) Taflove, A.; Hagness, S. C. *Computational Electrodynamics: The Finite-Difference Time-Domain Method*, 3rd ed.; Artech House: Boston, 2005.
(23) Dorfmüller, J.; Vogelgesang, R.; Weitz, R. T.; Rockstuhl, C.; Etrich, C.; Pertsch, T.; Lederer, F.; Kern, K. *Nano Lett.* **2009**, *9*, 2372–2377.
(24) Bohren, C. F.; Huffman, D. R. *Absorption and Scattering of Light by Small Particles*; Wiley-VCH: Weinheim, 1998.
(25) Pocklington, H. *Proc. Cambridge Philos. Soc.* **1897**, *9*, 461–461.
(26) Jones, D. S. The Theory of Electromagnetism; In *International Series of Monographs on Pure and Applied Mathematics*; Pergamon Press: Oxford, NY, 1964; Vol. 47
(27) Hallén, E. *J. Appl. Phys.* **1948**, *19*, 1140–1147.
(28) Ashley, J.; Emerson, L. *Surf. Sci.* **1974**, *41*, 615–618.
(29) Pfeiffer, C. A.; Economou, E. N.; Ngai, K. L. *Phys. Rev. B* **1974**, *10*, 3038–3051.
(30) Stratton, J. A. *Electromagnetic Theory*; McGraw-Hill: New York, 1941.
(31) *Antenna Engineering Handbook*; Volakis, J. L., Ed.; McGraw-Hill: New York, 2007.
(32) Gordon, R. *Opt. Express* **2009**, *17*, 18621–18629.
(33) Novotny, L. *Phys. Rev. Lett.* **2007**, *98*, 266802.
(34) Bancroft, R. *Microstrip and Printed Antenna Design*, 2nd ed.; SciTech Publishing Inc.: Raleigh, NC, 2009.
(35) Fumeaux, C.; Gritz, M.; Codreanu, I.; Schaich, W.; Gonzalez, F.; Boreman, G. D. *Infrared Phys. Technol.* **2000**, *41*, 271–281.
(36) Ghenuche, P.; Cherukulappurath, S.; Taminiau, T. H.; van Hulst, N. F.; Quidant, R. *Phys. Rev. Lett.* **2008**, *101*, 116805.
(37) Esteban, R.; Vogelgesang, R.; Dorfmüller, J.; Dmitriev, A.; Rockstuhl, C.; Etrich, C.; Kern, K. *Nano Lett.* **2008**, *8*, 3155–3159.
(38) Encina, E. R.; Coronado, E. A. *J. Phys. Chem. C* **2007**, *111*, 16796–16801.
(39) Johnson, P. B.; Christy, R. W. *Phys. Rev. B* **1972**, *6*, 4370–4379.
(40) Novotny, L.; Hecht, B. *Principles of Nano-Optics*; Cambridge University Press: Cambridge, 2006.
(41) Carson, J. R. *Bell. Syst. Tech. J.* **1924**, *3*, 393–399.
(42) Akimov, A. V.; Mukherjee, A.; Yu, C. L.; Chang, D. E.; Zibrov, A. S.; Hemmer, P. R.; Park, H.; Lukin, M. D. *Nature* **2007**, *450*, 402–406.
(43) Greffet, J.-J. *Science* **2005**, *308*, 1561–1563.
(44) Taminiau, T. H.; Stefani, F. D.; van Hulst, N. F. *physics.optics* **2009**, 1–10. *arXiv*.
(45) Encina, E. R.; Coronado, E. A. *J. Phys. Chem. C* **2008**, *112*, 9586–9594.
(46) Long, S. A.; McAllister, M. W.; Shen, L. C. *IEEE Trans. Antennas Propag.* **1983**, *31*, 406–412.
(47) Mongia, R. K.; Bhartia, P. *Int. J. Microw. Millimet. Wave Comput. Aided Eng.* **1994**, *4*, 230–247.

DOI: 10.1021/nl101921y | *Nano Lett.* **2010,** *10,* 3596–-3603